Communication

Tri-Port Antenna With Shared Radiator and Self-Decoupling Characteristic for 5G Smartphone Application

Bixia Yang, Yunxue Xu, Jiahao Tong, Yuhao Zhang, Yuwen Feng, and Yafei Hu

***Abstract*— A novel self-decoupling tri-port antenna is proposed. The three ports of the proposed antenna simultaneously excite a radiator printed on the inner surface of the smartphone frame. Based on the mode cancellation method and active reflection coefficient theory, the self-decoupling mechanism of the proposed antenna is investigated. The results reveal that the three ports remain well isolated and no decoupling structure is required. The simulated results illustrate that the isolation of the proposed tri-port antenna is higher than 11 dB in the LTE 42 band, and the envelope correlation coefficients (ECCs) are less than 0.14. A 12 × 12 multiple-input–multiple-output (MIMO) antenna system consisting of four tri-port antennas is designed, manufactured, and measured. The measured results show that the isolation among the 12 ports is better than 10 dB, and the ECCs are less than 0.14. The total efficiency of all ports is 51%–71%. The calculated channel capacity ranges from 57.98 to 59.87 bps/Hz when the signal-to-noise ratio (SNR) is 20 dB.**

***Index Terms*— Multiple-input–multiple-output (MIMO) antennas, self-decoupling, shared radiator, smartphone antenna, tri-port antenna.**

I. Introduction

Wireless communication technology has advanced considerably. The efficiency and reliability of communication systems have been improved markedly without an increase in the transmitting power and additional spectrum resources with the use of multiple-input–multiple-output (MIMO) technology [1]. For 5G mobile terminals, the miniaturization of MIMO antennas and performance improvement are critical topics of research.

The ergodic channel capacity within the existing bandwidth can be improved by increasing the number of elements of the MIMO array. MIMO arrays with 8, 12, and 16 elements have been reported [2]–[5]. A balanced slot antenna that produced a balanced slot mode was used in an eight-antenna array [2]. The channel capacity of the array was approximately 40 bps/Hz at 20 dB signal-to-noise ratio (SNR). Based on a tripolarized antenna module, a 12-antenna array achieved the channel capacity of approximately 57 bps/Hz at 20 dB SNR [4]. A 16-antenna array based on the quad-antenna linear (QAL) array achieved the channel capacity of 66 bps/Hz [5]. In these studies on MIMO antenna arrays of smartphones, one port excites one radiator. The array is large and occupies considerable space. Most designs require additional decoupling structures or specific antenna arrangements.

To compress the size of the MIMO array for use in size-limited mobile terminals, two solutions are currently used: in the first solution, multiple antennas are integrated to form a compact structure [5]–[10]; and in the second approach, a radiator is shared among antennas [3], [4], [11]–[13]. An asymmetric dual-port antenna based on an equivalent transmission line theory achieved high isolation and self-decoupling [3]. The neutralization line principle has been used to cancel the mutual coupling between adjacent slot antennas and folded monopole antennas [5], [6]. The coupling gap between the adjacent antenna and the lumped elements was used to form an LC tank to suppress the coupling between compact antennas [7], [8]. The lumped elements can be replaced with the distributed structure to achieve decoupling. A distributed LC tank was constructed by adjusting the coupling gap between the compact antenna pairs and the shorting band to suppress mutual coupling [9], [10]. In [11] and [12], the orthogonal mode was used to achieve excellent isolation without any decoupling structure. In [13], a novel method of mode cancellation based on differential mode (DM) and common mode (CM) was proposed and a simple double-fed, self-decoupled antenna pair was designed. Most compact structures consist of two antennas. Compact building blocks composed of four antennas have been proposed [5], [7], but these require additional decoupling and exhibit low efficiency. The size of the tripolarized antenna module proposed in [4] is relatively large ($17 \times 17 \times 6$ mm^3) and an additional neutralization line was required for decoupling between the top two modules.

In this communication, a self-decoupling tri-port antenna is proposed. The three ports of the proposed antenna simultaneously excite a radiator. Using the mode cancellation method, the self-decoupling characteristic between two symmetrical ports of the proposed antenna is analyzed. An active reflection coefficient theory is utilized to investigate the self-isolated mechanism between two asymmetric ports. The simulated results reveal that the isolation among the three ports of the proposed antenna is higher than 11 dB in the LTE 42 band, and the envelope correlation coefficients (ECCs) are less than 0.14. A 12 × 12 MIMO antenna system consisting of four tri-port antennas is designed, manufactured, and measured. The measured results reveal that the isolation among the 12 ports is better than 10 dB, and the ECCs are less than 0.14. The total efficiency is 51%–71%. A calculated channel capacity of 57.98–59.87 bps/Hz is achieved with 20 dB SNR.

II. Proposed Tri-Port Antenna

A. Construction of the Tri-Port Antenna

Fig. 1 shows the configuration of the proposed tri-port antenna. A metal ground (150×70 mm^2) is etched on the back face of the horizontal FR4 substrate ($\varepsilon r = 4.4$, $\tan\delta = 0.02$, and size: $150 \times 75 \times 0.8$ mm^3). A vertical FR4 substrate ($150 \times 7 \times 0.8$ mm^3) represents the frame of the smartphone. The antenna radiator (33×7 mm^2) is printed on the inner surface of the smartphone frame. The ground clearance is 2.5 mm away from the smartphone frame. The radiator is composed of two symmetrical U-shaped bent radiators with various arm lengths, and a 1 mm gap exists between the two U-shaped radiators. The feed microstrip lines of Ports 2 and 3

Manuscript received April 30, 2021; revised November 16, 2021; accepted November 18, 2021. Date of publication December 29, 2021; date of current version June 13, 2022. This work was supported by the National Natural Science Foundation of China under Grant 61401336 and Grant 61971335. *(Corresponding author: Yunxue Xu.)*

The authors are with the National Key Laboratory of Antennas and Microwave Technology, Xidian University, Xi'an 710071, China (e-mail: yunxuexu@sina.com).

Color versions of one or more figures in this article are available at https://doi.org/10.1109/TAP.2021.3137378.

Digital Object Identifier 10.1109/TAP.2021.3137378

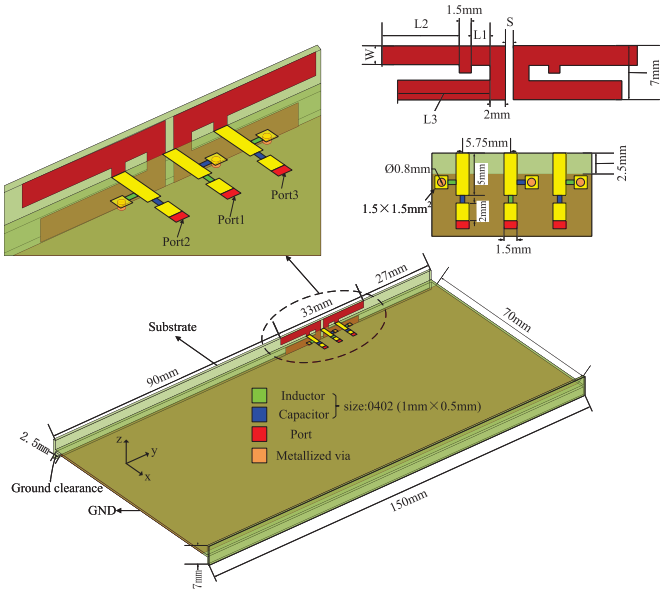

Fig. 1. Geometry of the proposed tri-port antenna. Detailed dimensions: L1 = 2.5 mm, L2 = 10 mm, L3 = 12 mm, s = 1 mm, and w = 2.5 mm.

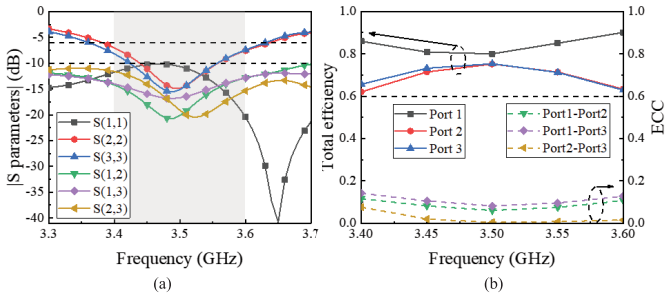

Fig. 2. Simulated performance of the proposed tri-port antenna. (a) S parameters. (b) Total efficiency and ECCs.

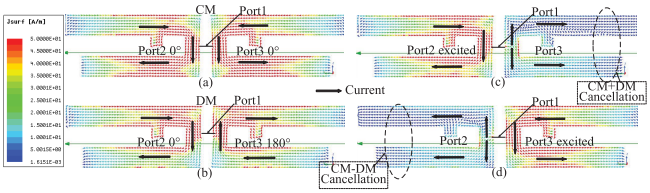

Fig. 3. Simulated vector surface current distributions at 3.5 GHz of the proposed tri-port antenna. (a) CM feed (Ports 2 and 3 are fed with equal amplitude and the same phase). (b) DM feed (Ports 2 and 3 are fed with equal amplitude and opposite phase). (c) Port2 excited. (d) Port3 excited.

are symmetrical about the gap and connected to the long arms of the two U-shaped bent radiators. The feed microstrip line of Port 1 is located in the gap and connected to two U-shaped bent radiators. Three 50 Ω feed microstrip lines with a width of 1.5 mm are printed on the upper surface of the horizontal FR4 substrate, and Γ-type impedance matching networks are introduced on the three feed ports. The series inductor and the shunt capacitor of the Γ-type impedance matching network of Port 1 are 1 nH and 0.7 pF, respectively. Because Ports 2 and 3 are symmetrical, the Γ-type impedance matching network of Port 2 is the same as Port 3, the shunt inductor is 1.7 nH, and the series capacitor is 0.4 pF.

B. Simulated Results of the Tri-Port Antenna

The simulated S parameters of the proposed tri-port antenna are shown in Fig. 2(a). The −10 dB impedance bandwidth of Port 1 is extremely wide, which exceeded the expected 3.4–3.6 GHz band. The −6 dB impedance bandwidth of Port 2 is 270 MHz, which covered the 3.37–3.64 GHz band. The −6 dB impedance bandwidth of Port 3 is 280 MHz, which covered the 3.35–3.63 GHz band. The isolation among the three ports is better than 11 dB during the 3.4–3.6 GHz band.

The diversity performance of the MIMO antenna system can be effectively evaluated by ECC. The simulated ECCs of the proposed tri-port antenna are shown in Fig. 2(b). The ECCs among the three ports are less than 0.14, leading to good diversity characteristic. As shown in Fig. 2(b), the simulated total efficiency of the proposed tri-port antenna reaches 59.6%–88.6%.

Although Ports 2 and 3 are symmetrical about the center gap of the radiator and their matching networks are the same, the curves in Fig. 2 are not completely consistent because the shunt capacitor of Port 1 is biased toward Port 3 (see Fig.1) and the antenna is not centered in the smartphone frame. The following difference of the curves of Ports 2 and 3 will not be repeated.

C. Working Principle of the Tri-Port Antenna

In [13], a mode cancellation method based on DM and CM was proposed for the symmetrical reciprocal dual-port antenna system, which theoretically proved that the mutual coupling between the symmetrical reciprocal dual-antenna system can be eliminated when CM and DM reflection coefficients are consistent with each other according to the following equation:

$$2|S_{21}| = |S_{cc11} - S_{dd11}|. \tag{1}$$

where S_{cc11} represents the CM reflection coefficient and S_{dd11} represents the DM reflection coefficient.

Thus, the good self-isolation characteristic between Ports 2 and 3 of the proposed tri-port antenna can be explained by the mode cancellation method. The CM and DM can be defined as a pair of orthogonal basis of a dual-port system [6], and Port 2 excitation can be equivalent to the superposition of DM and CM as follows:

$$I_2 = |I_{CM} + I_{DM}|. \tag{2}$$

Similarly, Port 3 excitation can be equivalent to a subtraction of CM and DM

$$I_3 = |I_{CM} - I_{DM}|. \tag{3}$$

Fig. 3 shows the simulated vector current distributions of the radiator of the proposed tri-port antenna at 3.5 GHz. Fig. 3(a) shows the current distribution of Ports 2 and 3 with equal amplitude and the same phase, that is, the CM current. Fig. 3(b) shows the current distribution when Ports 2 and 3 with equal amplitude and opposite phase, that is, the DM current. Fig. 3(c) shows the current distribution when Port 2 is excited and Port 3 is terminated with a 50 Ω load. The current distribution in Fig. 3(c) is the result of superimposition of the CM current [see Fig. 3(a)] and the DM current [see Fig. 3(b)]. Fig. 3(d) shows the current distribution when Port 3 is excited and Port 2 is terminated with a 50 Ω load. The current distribution in Fig. 3(d) is the subtraction of the CM current [see Fig. 3(a)] and the DM current [see Fig. 3(b)].

Fig. 4(a) shows the Smith chart of the CM and DM reflection coefficients of Ports 2 and 3 of the proposed tri-port antenna operating in 3.4–3.6 GHz band. According to [13], when Ports 1 and 2 perform $S_{21} < -10$ dB ≈ 0.316, then $|S_{cc11} - S_{dd11}| < 0.632$ (the normalized

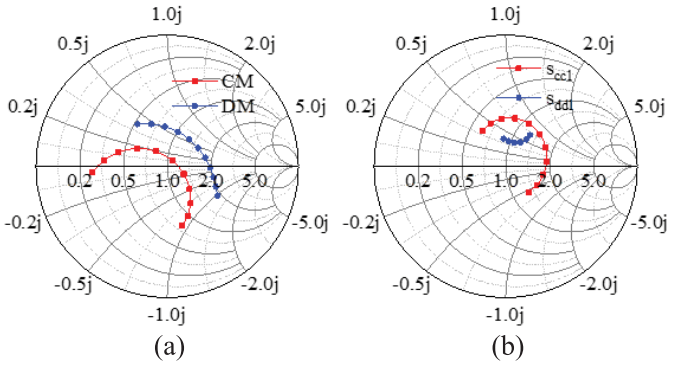

Fig. 4. Smith chart of (a) CM and DM reflection coefficients for Ports 2 and 3 of the proposed tri-port antenna operating in 3.4–3.6 GHz band. (b) s_{cc1} and s_{dd1} of the proposed tri-port antenna operating in 3.4–3.6 GHz band.

Smith chart). Fig. 4(a) shows that the curves of CM and DM are close, which satisfies our requirements.

Because Ports 2 and 3 are symmetrical and reciprocal dual-port networks, they can be analyzed by the mode cancellation theory. However, Ports 1 and 2 are asymmetric, which cannot be explained by this theory. Therefore, the active reflection coefficient theory is used to analyze the asymmetric dual-port network.

According to the theory of the scattering matrix [14]

$$\begin{bmatrix} b_1 \\ b_2 \end{bmatrix} = \begin{bmatrix} s_{11} & s_{12} \\ s_{21} & s_{22} \end{bmatrix} \begin{bmatrix} a_1 \\ a_2 \end{bmatrix} \tag{4}$$

where b_n represents the amplitude of the reflected wave from port n and a_n represents the amplitude of the incident wave from port n

$$\begin{bmatrix} s_{cc1} \\ s_{cc2} \end{bmatrix} = \begin{bmatrix} s_{11} & s_{12} \\ s_{21} & s_{22} \end{bmatrix} \begin{bmatrix} 1 \\ 1 \end{bmatrix} \tag{5}$$

$$\begin{bmatrix} s_{dd1} \\ s_{dd2} \end{bmatrix} = \begin{bmatrix} s_{11} & s_{12} \\ s_{21} & s_{22} \end{bmatrix} \begin{bmatrix} 1 \\ -1 \end{bmatrix} \tag{6}$$

where s_{ccn} is the active reflection coefficient of Port n when two ports are fed with equal amplitude and the same phase and s_{ddn} is the active reflection coefficient of the Port n when two ports are fed with equal amplitude and opposite phase. Thus, according to (5) and (6)

$$\begin{aligned} s_{cc1} &= s_{11} + s_{12}, \quad s_{cc2} = s_{21} + s_{22} \\ s_{dd1} &= s_{11} - s_{12}, \quad s_{dd2} = s_{21} - s_{22} \\ |s_{cc1} - s_{dd1}| &= 2|s_{12}|, \quad |s_{cc2} + s_{dd2}| = 2|s_{21}|. \end{aligned} \tag{7}$$

Thus, the mutual coupling between the asymmetric reciprocal dual-antenna system can be completely eliminated when s_{cc1} are the same with s_{dd1}. Fig. 4(b) shows the Smith chart of s_{cc1} and s_{dd1} of the proposed tri-port antenna operating in 3.4–3.6 GHz band. Fig. 4(b) shows that the curves of s_{cc1} and s_{dd1} are close, which satisfies our requirements.

The simulated vector surface current on the ground at 3.5 GHz of the proposed tri-port antenna is observed to investigate the good isolation of the three ports. As shown in Fig. 5, the current on the ground induced by Ports 1 and 2 is orthogonal, which effectively reduces the coupling from the ground [11].

Fig. 6 shows the Smith chart of the reflection coefficient before and after the addition of the matching network. The impedance matching of three ports improved after the addition of the matching network.

D. Parameter Scanning Analysis

Some critical parameter sweeps of the tri-port antenna design are shown in Fig. 7. Fig. 7(a) reveals that L1 considerably influences

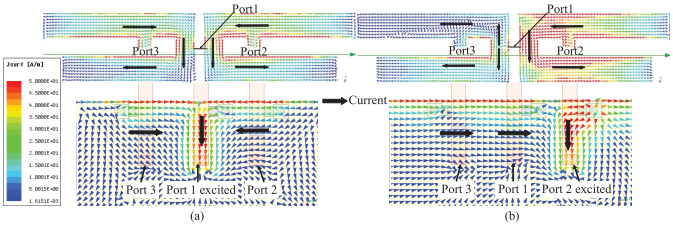

Fig. 5. Simulated vector surface current on the radiator and ground at 3.5 GHz of the proposed tri-port antenna. (a) Port 1 excited. (b) Port 2 excited.

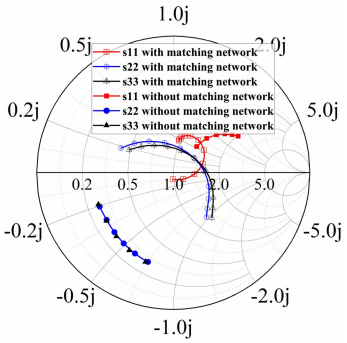

Fig. 6. Smith chart of the reflection coefficient before and after adding the matching network of the proposed tri-port antenna operating in 3.4–3.6 GHz band.

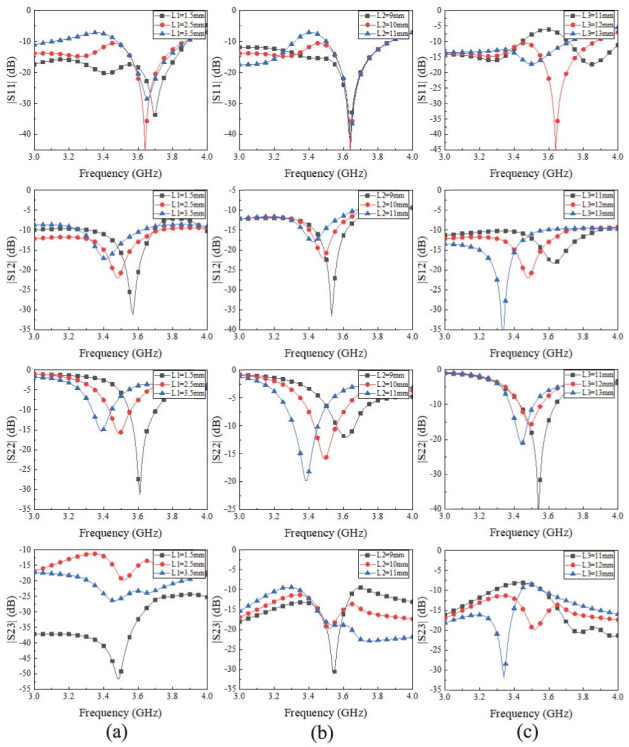

Fig. 7. Key parameter scanning on S parameter. The scanning of the parameter: (a) L1, (b) L2, and (c) L3.

S_{12} and S_{22}. As L1 increases, S_{12} and S_{22} shift to low frequencies with decreasing magnitude. L1 has a negligible effect on S_{11}, and L1 mainly affects the magnitude of S_{23}. As shown in Fig. 7(b), L2 has a negligible effect on S_{11} and S_{23}. As L2 increases, S_{12} shifts to low frequency with decreasing magnitude, and S_{22} shifts to low frequency with increasing magnitude. Fig. 7(c) shows the vital parameter L3.

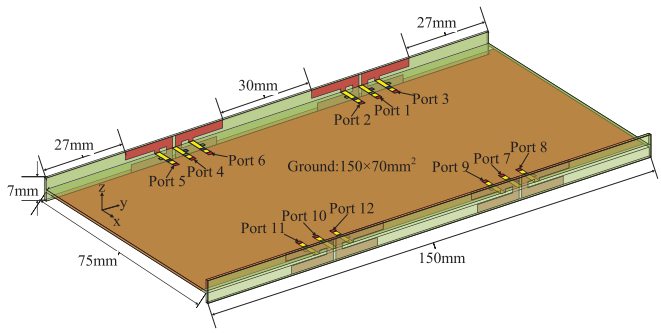

Fig. 8. Details of the proposed 12 × 12 MIMO antenna system.

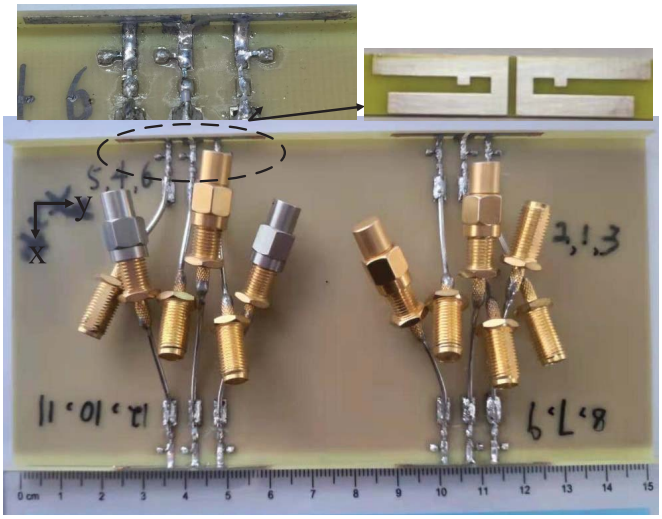

Fig. 9. Photograph of the prototype of the proposed 12 × 12 MIMO antenna system.

All S parameters are affected by L3. As L3 increases, all S parameters shift to low frequency.

Thus, the optimization process can be summarized as follows. First, S_{23} is optimized by L3, and S_{12} and S_{13} are mainly adjusted by L1 and L2. Finally, the matching network is added to improve impedance matching.

III. Proposed 12 × 12 MIMO Antenna System

A. Geometry and Fabrication of the 12 × 12 MIMO Antenna System

Fig. 8 shows a schematic of the proposed 12 × 12 MIMO antenna system. A metal ground (150 × 70 mm^2) is etched on the back face of the horizontal FR4 substrate (εr = 4.4, tan δ = 0.02, and size: 150 × 75 × 0.8 mm^3). The vertical FR4 substrate (150 × 7 × 0.8 mm^3) represents the frame of the smartphone. Four tri-port antennas are symmetrically distributed on the inner surface of the frame, and the distance between the two antennas on the same side is 30 mm to obtain acceptable isolation. The ground clearance is 2.5 mm away from the edge of the frame of the smartphone. Fig. 9 shows the photograph of the fabricated 12 × 12 MIMO antenna system. Twelve 50 Ω semirigid cables are connected to 12 ports for testing.

B. Performance of the Simulation and Measurement

The simulated and measured reflection coefficients of the proposed 12 × 12 MIMO antenna system are shown in Fig. 10(a). Since the 12 × 12 MIMO antenna system is composed of four tri-port antennas with mirror symmetry, the results of Ports 4–12 are not listed. The simulated and measured reflection coefficients of the three ports in the 3.4–3.6 GHz band are all less than −6 dB. The slight deviation of frequency between simulation and measurement is caused by manufacturing errors and test cables. The measurement result of Port 1 differed marginally from the simulation result because of manual errors.

TABLE I

Measured Gain of the Proposed Tri-Port Antenna, Unit: dBi

Freq [GHz]	Port 1	Port 2	Port 3
3.4	4.66	2.53	2.36
3.5	3.16	3.66	3.41
3.6	3.11	2.34	2.55

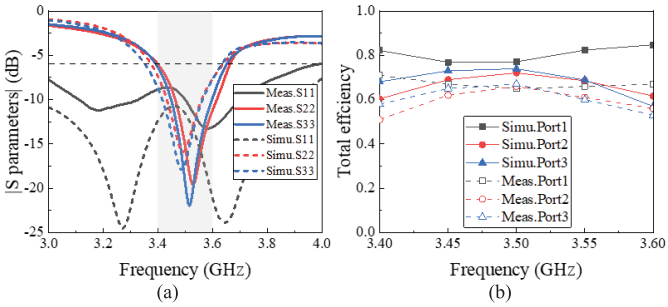

Fig. 10. Simulated and measured (a) reflection coefficients and (b) total efficiency of the proposed 12 × 12 MIMO antenna system.

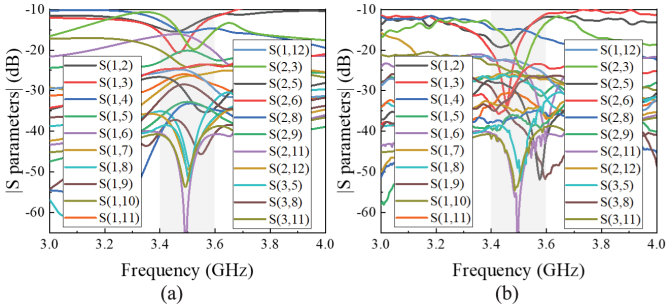

Fig. 11. Isolation of the proposed 12 × 12 MIMO antenna system. (a) Simulated. (b) Measured.

The simulated and measured total efficiencies are shown in Fig. 10(b). The simulated and measured total efficiencies of Port 1 are 76.9%–84.8% and 65.0%–71.0%, respectively; the simulated and measured total efficiencies of Port 2 are 60.4%–72.1% and 51%–66%, respectively; the simulated and measured total efficiencies of Port 3 are 57.0%–74.0% and 53.0%–67.0%, respectively. The measured total efficiency is lower than the simulated total efficiency probably because of the loss of the lumped element and coaxial line.

Fig. 11 shows the simulated and measured transmission coefficients of the proposed 12 × 12 MIMO antenna system. Fig. 11(a) and (b) shows that the isolation among 12 ports is higher than 10 dB.

Fig. 12 shows the simulated and measured radiation patterns of the three ports on phi = 0°, phi = 90°, and theta = 90° at 3.5 GHz. The trends of the simulation and measurement curves are coincident, which verifies the feasibility of this structure.

The measured antenna gains are listed in Table I. The antenna gain is 3.11–4.66 dBi when Port 1 is excited, 2.34–3.66 dBi when Port 2 is excited, and 2.36–3.41 dBi when Port 3 is excited.

TABLE II
COMPARISON BETWEEN THE PROPOSED TRI-PORT ANTENNA AND THE EXISTING LITERATURE

Ref.	Center Freq.(GHz)	Decoupling mechanism	Port	Size(mm^3)	Isolation (dB)	ECC	Efficiency(%)
[4]	3.5	Tri-Polarized	3	17×17×6	>12.5	<0.2	>50
[11]	3.5	mode orthogonality	2	28.4×1×0.5	>16	<0.05	>50
[12]	3.5/4.5	mode orthogonality	2	40×7.5×3	>21/>12	<0.11	>58.9/>31.6
[13]	3.75	Self-decoupled	2	30×7.5×2	>10.5	<0.2	>63.1
Proposed	3.5	Self-decoupled	3	33×7×2.5	>11	<0.14	>51

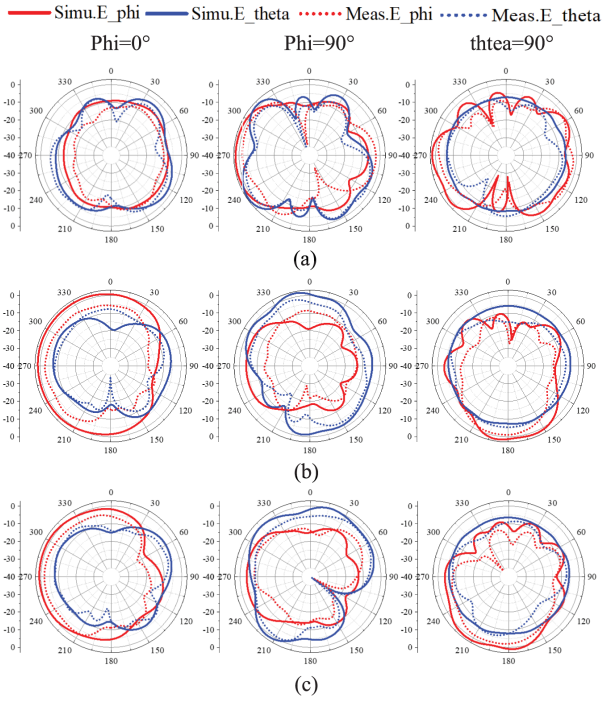

Fig. 12. Simulated and measured radiation patterns of three ports on phi = 0°, phi = 90°, and theta = 90° at 3.5 GHz. (a) Port 1. (b) Port 2. (c) Port 3.

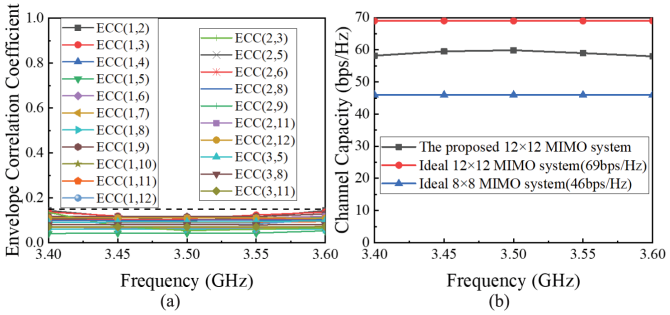

Fig. 13. MIMO performance that calculated by the measured complex far field of the proposed 12 × 12 MIMO antenna system. (a) ECC. (b) Ergodic channel capacity.

C. MIMO Performance

The diversity performance of the MIMO antenna system can be effectively evaluated using ECC, which can be obtained by analyzing the complex far-field pattern [13]. Fig. 13(a) shows the measured ECCs of the proposed 12 × 12 MIMO antenna system and reveals that the ECCs are lower than 0.14. A higher diversity gain typically benefits from lower ECCs, and the acceptable value for ECC is less than 0.5 [2]. The proposed 12 × 12 MIMO antenna system adequately satisfied the acceptable standard.

To verify the multiplexing capability of the proposed 12 × 12 MIMO antenna system, the ergodic channel capacity is evaluated. The calculation formula of the ergodic channel capacity without considering the channel state information of the transmitter was provided [15]. By averaging 10 000 random Rayleigh fading channels at 20 dB SNR, the calculated ergodic channel capacity of the proposed 12 × 12 MIMO antenna system is obtained in Fig. 13(b). The calculated ergodic channel capacity of the proposed 12 × 12 MIMO antenna system reaches 57.98–59.87 bps/Hz in the operating band, which is marginally lower than the ideal 12 × 12 MIMO antenna system (69 bps/Hz) and higher than the ideal 8 × 8 MIMO antenna system (46 bps/Hz). The high channel capacity of the proposed tri-port antenna means superior multiplexing capability and its potential to be used in 5G mobile phone applications.

IV. COMPARISON

Table II presents a comparison between the proposed tri-port antenna and previous studies. In most of the previous studies, two ports share a radiator [11]–[13], which restricts the placement of more MIMO antennas. Although a tripolarized antenna module was introduced [4], the 12 × 12 MIMO antenna array was realized by placing four tripolarized antenna modules on the four corners of the smartphone. However, the size of the tripolarized antenna modules was large (17 × 17 × 6 mm^3), and an additional neutralization line was required for decoupling the top two modules. Therefore, the module is not suitable for current popular smartphones with large screens and narrow bezels. In this communication, a novel tri-port antenna with a symmetrical planar structure is proposed. The simplicity, compactness, self-decoupling, and high efficiency of the proposed antenna render it a promising material in highly integrated 5G mobile communications.

V. CONCLUSION

A novel tri-port antenna with self-decoupling characteristic and shared radiator is proposed. Using the orthogonality of the mode cancellation method based on DM and CM, the self-decoupling characteristic between two symmetrical ports is analyzed. An active reflection coefficient theory is used to explain the self-isolated mechanism between two asymmetric ports. The simulated results reveal that the isolation among the three ports is higher than 11 dB in the 3.4–3.6 GHz band, and the ECCs are less than 0.14. A 12 × 12 MIMO antenna system consisting of four tri-port antennas is designed, manufactured, and measured. The measured results display that the isolation among the 12 ports is higher than 11 dB in the 3.4–3.6 GHz band, the ECCs are less than 0.14, and the total

efficiency is 51%–71%. The calculated channel capacity with 20 dB SNR reaches 57.98–59.87 bps/Hz. Therefore, the proposed 12 × 12 MIMO antenna system could be used in 5G mobile communications because of its acceptable isolation, compact size, self-decoupling characteristics, and high efficiency.

REFERENCES

[1] E. G. Larsson, O. Edfors, F. Tufvesson, and T. L. Marzetta, "Massive MIMO for next generation wireless systems," *IEEE Commun. Mag.*, vol. 52, no. 2, pp. 186–195, Feb. 2014, doi: 10.1109/MCOM.2014.6736761.

[2] Y. Li, C.-Y.-D. Sim, Y. Luo, and G. Yang, "High-isolation 3.5 GHz eight-antenna MIMO array using balanced open-slot antenna element for 5G smartphones," *IEEE Trans. Antennas Propag.*, vol. 67, no. 6, pp. 3820–3830, Jun. 2019, doi: 10.1109/TAP.2019.2902751.

[3] B. Yang, Y. Xu, F. Lu, R. Li, L. Zhang, and Y. Liu, "High-isolation dual-port antenna with self-decoupling characteristics for 5G smartphone applications," *Int. J. RF Microw. Comput.-Aided Eng.*, vol. 31, no. 8, Aug. 2021, Art. no. e22702, doi: 10.1002/mmce.22702.

[4] M.-Y. Li, Y.-L. Ban, Z.-Q. Xu, J. Guo, and Z.-F. Yu, "Tri-polarized 12-antenna MIMO array for future 5G smartphone applications," *IEEE Access*, vol. 6, pp. 6160–6170, 2018, doi: 10.1109/ACCESS.2017.2781705.

[5] K. L. Wong, J.-Y. Lu, L.-Y. Chen, W.-Y. Li, and Y.-L. Ban, "8-antenna and 16-antenna arrays using the quad-antenna linear array as a building block for the 3.5-GHz LTE MIMO operation in the smartphone," *Microw. Opt. Technol. Lett.*, vol. 58, no. 1, pp. 174–181, Jan. 2016.

[6] L. Sun, Y. Li, and Z. Zhang, "Wideband decoupling of integrated slot antenna pairs for 5G smartphones," *IEEE Trans. Antennas Propag.*, vol. 69, no. 4, pp. 2386–2391, Apr. 2021, doi: 10.1109/TAP.2020.3021785.

[7] C. Deng, D. Liu, and X. Lv, "Tightly arranged four-element MIMO antennas for 5G mobile terminals," *IEEE Trans. Antennas Propag.*, vol. 67, no. 10, pp. 6353–6361, Oct. 2019, doi: 10.1109/TAP.2019.2922757.

[8] K.-L. Wong and L.-Y. Chen, "Dual-inverted-F antenna with a decoupling chip inductor for the 3.6-GHz LTE operation in the tablet computer," *Microw. Opt. Technol. Lett.*, vol. 57, no. 9, pp. 2189–2194, 2015, doi: 10.1002/mop.29288.

[9] K.-L. Wong, C.-Y. Tsai, and J.-Y. Lu, "Two asymmetrically mirrored gap-coupled loop antennas as a compact building block for eight-antenna MIMO array in the future smartphone," *IEEE Trans. Antennas Propag.*, vol. 65, no. 4, pp. 1765–1778, Apr. 2017, doi: 10.1109/TAP.2017.2670534.

[10] Z. Ren, A. Zhao, and S. Wu, "MIMO antenna with compact decoupled antenna pairs for 5G mobile terminals," *IEEE Antennas Wireless Propag. Lett.*, vol. 18, no. 7, pp. 1367–1371, Jul. 2019, doi: 10.1109/LAWP.2019.2916738.

[11] A. Ren, Y. Liu, and C.-Y.-D. Sim, "A compact building block with two shared-aperture antennas for eight-antenna MIMO array in metal-rimmed smartphone," *IEEE Trans. Antennas Propag.*, vol. 67, no. 10, pp. 6430–6438, Oct. 2019, doi: 10.1109/TAP.2019.2920306.

[12] L. Sun, Y. Li, Z. Zhang, and Z. Feng, "Wideband 5G MIMO antenna with integrated orthogonal-mode dual-antenna pairs for metal-rimmed smartphones," *IEEE Trans. Antennas Propag.*, vol. 68, no. 4, pp. 2494–2503, Apr. 2020, doi: 10.1109/TAP.2019.2948707.

[13] L. Sun, Y. Li, Z. Zhang, and H. Wang, "Self-decoupled MIMO antenna pair with shared radiator for 5G smartphones," *IEEE Trans. Antennas Propag.*, vol. 68, no. 5, pp. 3423–3432, May 2020, doi: 10.1109/TAP.2019.2963664.

[14] D. M. Pozar, *Microwave Engineering*, 2nd ed. New York, NY, USA: Wiley, 1998.

[15] R. Tian, B. K. Lau, and Z. Ying, "Multiplexing efficiency of MIMO antennas," *IEEE Antennas Wireless Propag. Lett.*, vol. 10, pp. 183–186, 2011, doi: 10.1109/LAWP.2011.2125773.